

Classical simulations of heavy-ion collisions

T. J. Schlagel and V. R. Pandharipande

Department of Physics, University of Illinois at Urbana-Champaign, Urbana, Illinois 61801

(Received 22 December 1986)

We have carried out simulations of central collisions between two heavy ions by the classical molecular dynamics method. The ions used in these simulations are bound spheres of charged argon atoms, and the chosen mass numbers for the collisions are 108 on 108, 65 on 65, and 16 on 200. A few hundred collisions are studied for five energies chosen to span fusion-fission, multifragmentation, and total vaporization reactions. We have also studied the disassembly of hot liquid drops containing 216 and 130 particles. By comparing collisions and disassembly we establish the formation of equilibrated hot matter in the collisions. The density of the hot matter formed appears to be $\sim 80\%$ of the equilibrium density, and its temperature depends upon the beam energy. All the beam energy thermalizes in equal mass collisions; however, a large fraction of it is lost in pre-equilibrium emission in the asymmetric 16 on 200 collisions. Mass yields and energy spectra of the particles emitted in collisions and disassemblies are reported, and the role of the liquid-gas phase transition is discussed. The yield of small clusters having $A_c < 30$ particles is approximately given by the $A_c^{-\tau_{\text{eff}}}$ power law. The τ_{eff} depends on the energy of the collision, and has a minimum value of ~ 1.7 as observed in nuclear fragmentation reactions.

I. INTRODUCTION

Fragmentation of nuclei has been observed in many nuclear reactions.¹⁻³ A microscopic theory of these reactions is very difficult due to the quantum nature of nuclei, particularly the Fermi statistics, and the exchange character of nuclear forces. Treatments of these reactions, based on quantum mechanics,⁴⁻⁶ generally assume that the particles move in an average potential determined from the local density and kinetic energy, and solve either the time dependent Hartree-Fock, or Vlasov, equations. It is also possible to consider pairwise collisions via the Boltzmann-Uehling-Uhlenbeck⁷ formalism. Simple thermodynamic arguments, independent of either the quantum nature or the details of nuclear forces, are also used to discuss these reactions, with the hope that the macroscopic equation of state and the liquid-gas phase transition play an important role. In the simplest model^{8,9} of fragmentation reactions one assumes the formation of a hot compound nucleus that cools as it expands. If the density and temperature of the expanding matter attain values at which the compressibility becomes negative, then large density fluctuations can develop and break the nucleus into several pieces. The mean field theories, based on an average single particle potential determined by local density and kinetic energy, implicitly assume that the reaction depends most strongly on the equation of state.

Because of the dynamic nature of these reactions and the small number of particles involved, it is not obvious that we can use equilibrium thermodynamics to describe them. However, if thermodynamic arguments do apply, then they should also apply to classical systems whose reactions can be calculated exactly by solving Newton's equations of motion. With this point of view Vicentini, Jacucci, and Pandharipande¹⁰ studied the fragmentation of hot drops containing ~ 200 argon atoms using the

molecular dynamics method. They found four modes of disassembly starting from ordinary evaporation at the lowest energies (or initial temperatures), to violent evaporation, fragmentation, and total vaporization at very high energies. Violent evaporation occurs when e , the total energy per particle, is negative, but the excitation energy is a large fraction of the binding energy. In this energy range the drops expand into the region of adiabatic instabilities and develop density fluctuations. For e sufficiently negative, the expansion stops when the average density is greater than $0.2\rho_L$, where ρ_L is the liquid density. At this stage the system stays connected, and resembles a liquid drop of rather crooked shape. The large excess surface energy is evaporated away and the drop relaxes back to a spherical shape. When $e > 0$, the expansion continues to average densities less than $0.2\rho_L$, and the system fragments into several pieces. The largest fragments were found when $e \sim 0$. At very high energies the expanding matter never reaches the region of adiabatic instabilities and the system totally vaporizes without leaving large fragments. These studies showed that fragmentation of even 100- to 200-particle systems is intimately connected to the existence of a liquid-gas transition.

Following this work, Lenk and Pandharipande¹¹ studied the fragmentation of hot charged liquid drops by adding a fictitious Coulomb potential between argon atoms. The strength of this potential was chosen so that the binding energy formula of argon granules resembled the nuclear liquid drop mass formula. They found that the Coulomb interaction does not have a large effect on the vaporization or fragmentation modes of disassembly, but the violent evaporation mode is strongly affected. When the system expands and recondenses it generally picks up a deformation. The Coulomb forces exploit these deformations, and produce, in systems with ~ 200 particles, copious binary fission at low energies, and multiple fission

at higher energies.

Following this work we have carried out molecular dynamics calculations of head on collisions between cold charged argon balls containing A_1 and A_2 particles. The chosen values of (A_1, A_2) are (108,108), (200,16), and (65,65). We have also studied the disassembly of hot drops containing 216 and 130 particles at two initial densities. The collisions and disassemblies are calculated at five energies chosen to study binary fission, multiple fission, fragmentation, and vaporization. Typically, 100 events of each case are studied to obtain a reasonable idea of mass, energy, and angular distributions in the final state. The calculation details are given in Sec. II, while the dynamics of the collisions are discussed in Sec. III. The mass yields, energy distributions, and angular distributions are given in Secs. IV, V, and VI, respectively, and the results are discussed in Sec. VII.

II. THE CALCULATIONS

The time evolution is calculated with the molecular dynamics method¹⁰ using the Hamiltonian

$$H = \sum_{i=1, A} \frac{p_i^2}{2m} + \sum_{i < j \leq A} v(r_{ij}) + q^2/r_{ij}, \quad (2.1)$$

where $A (= A_1 + A_2)$ is the total number of particles in the system, $v(r_{ij})$ is a truncated Lennard-Jones 6,12 potential,

$$v(r < 3) = 4(r^{-12} - r^{-6}) - 4(3^{-12} - 3^{-6}), \quad (2.2)$$

$$v(r > 3) = 0, \quad (2.3)$$

and q^2/r_{ij} is a fictitious Coulomb interaction. The natural units for length and energy of the argon interatomic potential are 3.405 Å and 119.8 K, and we use $q^2 = 0.055$ in these units. Neutral matter is defined, as is nuclear matter, by switching off the Coulomb potential. The equation of state of neutral matter is given in Ref. 10; its phase diagram is similar to that of nuclear matter, apart from the existence of the solid phase. The solid phase does not seem to have a significant effect on problems studied here.

We study collisions between two cold glassy (i.e., not crystalline) balls of argon. The balls are made by cutting spheres, containing the required number of particles, out of equilibrated liquid at high temperature. The velocities of the particles are set to zero (quenched), and the sphere is evolved for a short time (generally $\sim 50 \times 10^{-14}$ s). The velocities are then quenched again. This process is repeated until the system has reached a local glassy equilibrium.

Head on collisions are studied by setting two glassy balls at zero temperature sufficiently apart, with velocities along the line joining their centers of mass, and calculating their time evolution. The disassembly of a hot liquid drop is studied, as in Refs. 10 and 11, by putting a spherical drop of equilibrated liquid in vacuum at time $t = 0$. The microscopic initial states of the collision or disassembly events are different even when their macroscopic states are the same. The macroscopic variables for collision events are A_1 , A_2 , and the center of mass beam energy, while for disassembly events they are A , the initial densi-

ty, and the initial temperature. Every simulated event is microscopically independent, and has a different final state. A large (few hundred) number of events with identical macroscopic initial conditions are used to study probability distributions in the final state. The total energy is not considered a macroscopic variable, and thus it is not exactly the same in all events. The fluctuations in e in collision events come from fluctuations in the binding energy of glass balls and are negligible, while those in disassembly events are statistical and are $\sim 10\%$.

The value of the Coulomb charge q was obtained in Ref. 11 by comparing the binding energy formula for argon balls with the nuclear liquid drop mass formula. The volume and surface energies were obtained from crystalline argon with the untruncated Lennard-Jones 6,12 potential. A more accurate binding energy formula can now be obtained by fitting the calculated energies ($e = E/A = -3.686$, -3.919 , and -3.880) of balls having $A = 200$, 108, and 65. Using $E/A = -7.94$ for the extended solid with the truncated potential (in contrast, the full potential gives -8.3), we obtain

$$e = -7.94 + 12.2 A^{-1/3} + 0.0638 A^{2/3}. \quad (2.4)$$

We stress that the classical argon balls used in this study are not intended to be mock nuclei, but instead to provide simple systems whose time evolution can be studied exactly by solving Newton's equations of motion. Direct comparisons with nuclear data are difficult. The natural unit of length is approximately the mean interparticle distance at equilibrium. Thus the natural length unit for nuclear matter should be ~ 1.8 fm. However, with this unit of length the nucleon-nucleon scattering cross section is ~ 1 , while that for argon-argon scattering is ~ 3 . The natural energy unit may be defined as $\sim \frac{1}{8}$ th the binding energy of neutral matter. It then is ~ 2 MeV for nuclear matter, and the incompressibility, binding energy, and liquid-gas critical temperature are ~ 115 , 8, and 9 for nuclear matter and ~ 300 , 8, and 1.3 for atomic argon matter. The critical temperature of nuclear matter is large due to its quantum nature. The unit of time in the simulations is 10^{-14} s. The time required for sound to travel a unit length in liquid argon is $\sim 4 \times 10^{-13}$ s, or 40 time steps. The time required by sound to travel a unit distance (1.8 fm) in nuclear matter is $\sim 10^{-23}$ s or 0.3 fm/c. The fragmentation reactions are quite slow; they typically take 500–10 000 time steps, and hence it is expected that equilibrium thermodynamics can be used to study them.

It is possible to define a classical system such that its density, binding energy and compressibility are similar to nuclear matter. Classical potentials that give reasonable two-body cross section and simulate the quantum Fermi kinetic energy have also been studied.^{12,13}

III. DYNAMICS OF THE COLLISIONS

The time evolution of the particles in two 108-on-108 collision events is shown in Figs. 1(a)–1(e) and 2(a)–2(c). The initial momenta are along the Z axis, and the Y axis is chosen to exhibit the dynamics of the collision most clearly. The $+$ and \circ denote the Y, Z coordinates of the

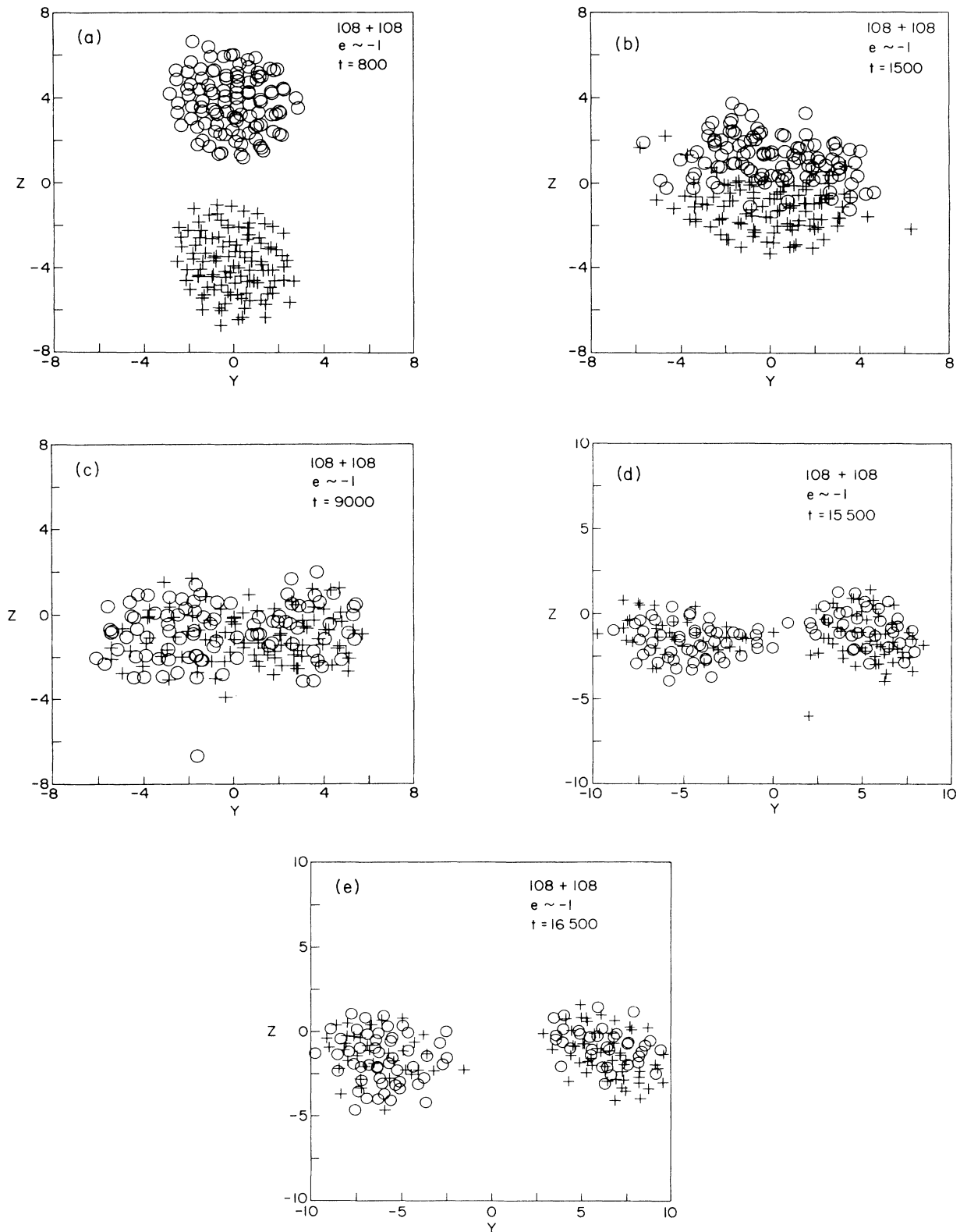


FIG. 1. Panels (a)–(e) show the Y and Z coordinates of particles, at chosen time intervals, in a $108 + 108$ collision at $e \sim -1$. The positions of particles in one of the balls are denoted by $+$, while \circ 's denote the positions of particles from the other ball. The beam axis is Z , and the Y axis is chosen such that the fission fragments are in the Y - Z plane. The compound system forms at $t \sim 800$ steps, and breaks up at $t \sim 15500$ steps. Note that the fission fragments are well separated by $t \sim 16500$, and they contain a mixture of particles from both the balls.

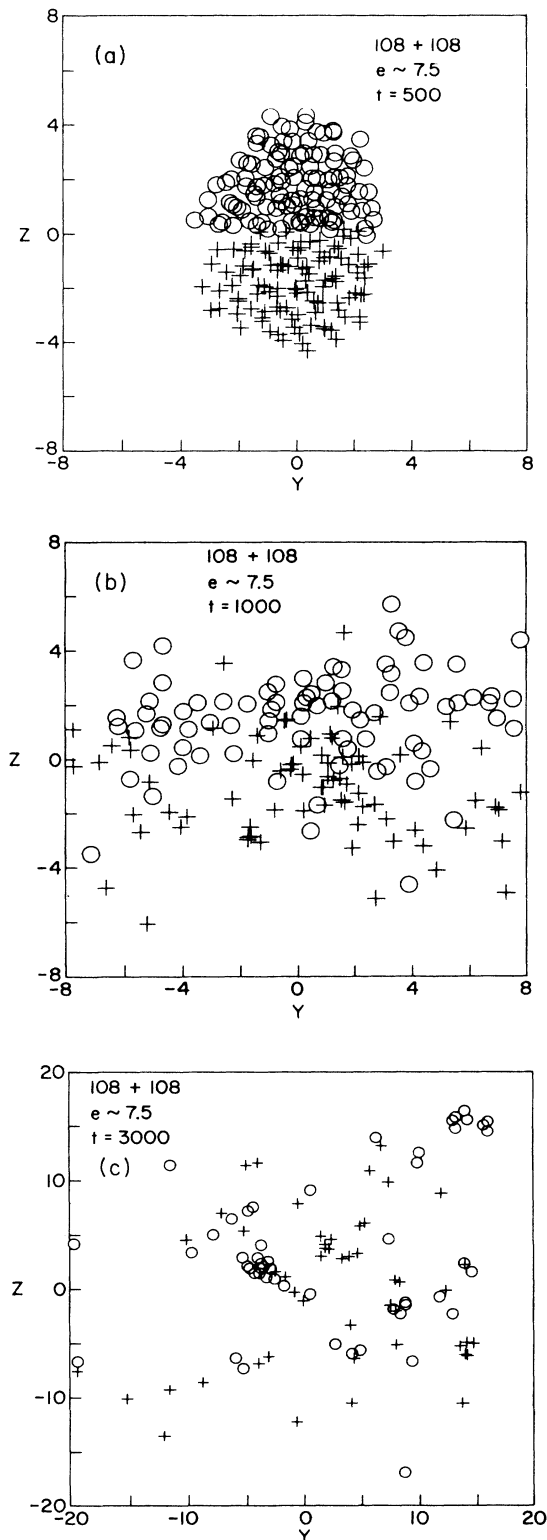


FIG. 2. Panels (a)–(e) show the Y and Z coordinates of particles in a $108 + 108$ collision at $e \sim 7.5$. See caption of Fig. 1 for details. Some of the smaller clusters produced in these collisions are made up of particles from only one of the balls, while some contain a mixture of particles from both balls.

particles from each of the colliding balls. The event shown in Figs. 1(a)–1(e) has a total energy $e \sim -1$ per particle which includes the -3.67 per particle binding energy of the balls. The energies given here are averages of many events with the same macroscopic initial state. In a fixed target experiment this corresponds to a lab energy of 10.7 per particle. It is a “low energy” event with respect to the energy range considered in this work, and results in a binary fission. We note that e must be greater than -3 to overcome the Coulomb barrier in a 108 -on- 108 collision. The “high energy” event shown in Figs. 2(a)–2(c) has $e \sim 7.5$, or a fixed target lab energy of 44.8 per particle, and it essentially produces a total vaporization of both the balls. The time evolution of the $e \sim -1$ event is much slower than that of the $e \sim 7.5$ event. The long time scales make it difficult to study the events at much lower energies. We note that there is a rather complete mixing of the particles from the two colliding balls, and in the case of the $e \sim -1$ event the compound system lives for an appreciable time. In both events there is a flattening of the particle distribution in the $Z = 0$ plane, and as a result the angular distribution of the collision products is peaked at $\theta = 90^\circ$. The angular distributions are discussed in Sec. VI.

A cluster of particles is defined¹⁰ so that it is possible to go from any particle of the cluster to another particle in the cluster by successive interparticle jumps of distance < 3 . Thus particles in a cluster interact with particles outside of the cluster or other clusters by only Coulomb force. Initially there are two cold clusters that have small internal energy and large center of mass energy. When these clusters collide they form a single cluster that has no center of mass energy, and its internal energy is e per particle. This cluster is called the compound system, and it can lose its internal energy by evaporation, emission of small fragments, etc. In Figs. 3 and 4 we show the variation of the internal energy of the compound system formed in $108 + 108$ and $200 + 16$ collisions at various energies. We note that the compound system formed in $200 + 16$ collisions loses its energy much faster than that

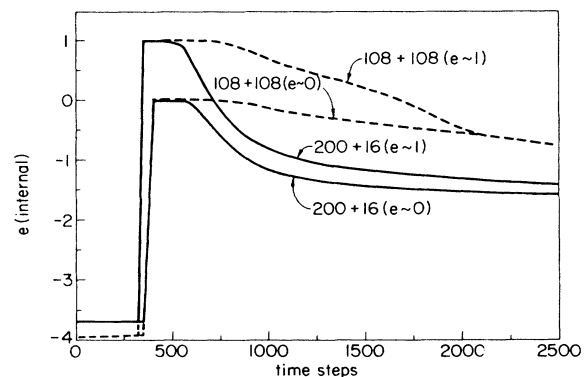
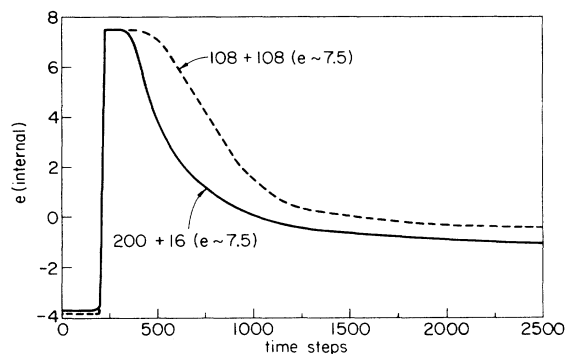


FIG. 3. The internal energy of the compound system formed in $108 + 108$ and $200 + 16$ collisions at $e \sim 0$ and 1 is shown as a function of time. The sudden increase in internal energy marks the beginning of the collision.

FIG. 4. Same as Fig. 3, except at $e \sim 7.5$.

in 108 + 108 collisions. From the comparison of the evolution trajectories, mass yields, and energy spectra observed in collisions and the disassembly of equilibrated hot drops, it appears that most of the collision energy in 108 + 108 and 65 + 65 collisions thermalizes, but in 200 + 16 collisions only a fraction of it thermalizes. A significant amount of the collision energy is lost in pre-equilibrium emission in 200 + 16 collisions, and the spectrum of single particles (Sec. V) emitted in these collisions has a high energy tail.

Let the largest cluster have N_L particles; the compound system has all the $A = A_1 + A_2$ particles in it when the reaction begins, and until fission or fragmentation it is the largest cluster. The $N_L/2$ particles closest to the center of mass of the largest cluster are called central particles. The average central density ρ_{ac} is defined as

$$\rho_{ac} = \frac{3N_L}{8\pi R_c^3}, \quad (3.1)$$

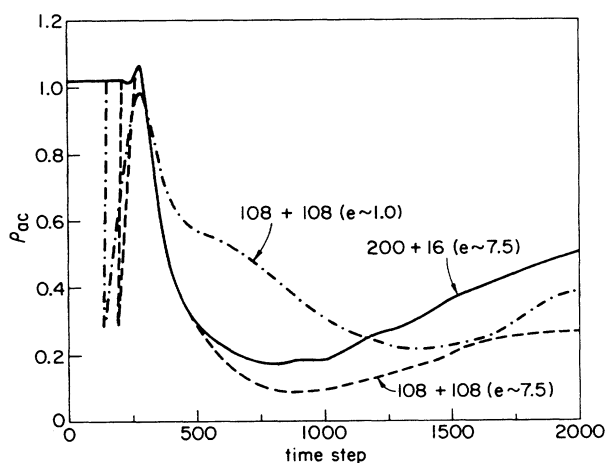


FIG. 5. The variation of the average central density ρ_{ac} in 108 + 108 ($e \sim 1$ and 7.5) and 200 + 16 ($e \sim 7.5$) collisions is shown by dashed-dotted, dashed, and solid curves. The sudden decrease of ρ_{ac} in 108 + 108 collisions marks the formation of a compound cluster. In 200 + 16 collisions the ρ_{ac} does not change rapidly when the clusters touch because the center of mass is inside the 200-body cluster.

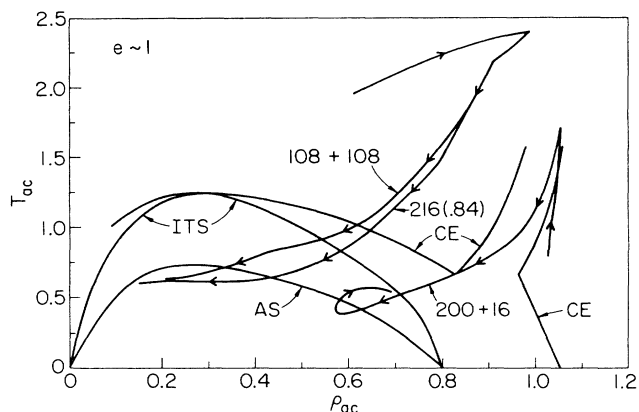


FIG. 6. The evolution trajectories of central matter in 108 + 108 and 200 + 16 collisions at $e \sim 1$ are compared with that of central matter in the expansion of hot 216-body drops from an initial temperature of 1.8, density 0.84, and average energy $e \sim 1$ [curve marked 216(0.84)]. The coexistence, isothermal spinodal, and adiabatic spinodal curves of the phase diagram of extended matter are labeled CE, ITS, and AS, respectively.

where R_c is the radius of the smallest sphere that contains all the central particles. Figure 5 shows the time evolution of ρ_{ac} in 108 + 108 collisions. Initially, either one of the cold 108-body clusters is the largest, and ρ_{ac} is its central density; it equals the equilibrium density of 1.04 for the glassy phase. When the reaction begins the entire system becomes a single cluster with its center of mass at the point where the surfaces of the two balls touch. At this time the ρ_{ac} becomes small due to this relocation of the center of mass. It then increases as the two clusters collide; however, it never exceeds 1.1. Thus in the energy range considered here we do not see any compression of matter. In fact, it appears that the compound system behaves as a hot drop of liquid at density of ~ 0.84 .

The average central temperature is defined as

$$T_{ac} = \frac{2}{N_L} \sum_{\text{central particles } i} \frac{1}{2} m v_i^2(i), \quad (3.2)$$

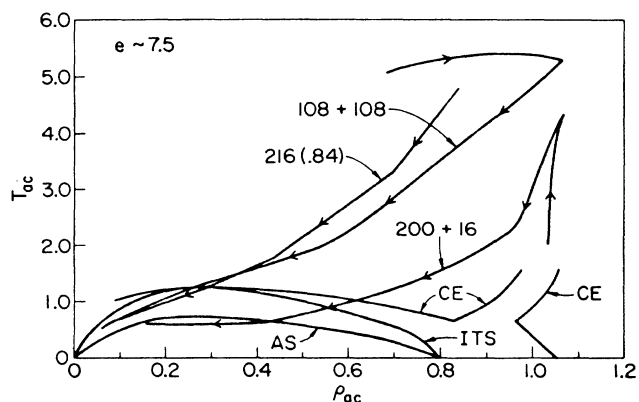


FIG. 7. Same as Fig. 6, except at $e \sim 7.5$.

where $v_{\perp}(i)$ is the velocity of the particle i perpendicular to its radius vector \mathbf{r}_i from the center of mass. When matter is in thermal equilibrium, T_{ac} equals its temperature, even when it is isotropically expanding. By taking v_{\perp} one gets rid of the collective motion of expansion.¹⁰ The plots of T_{ac}, ρ_{ac} parametric in time are called evolution trajectories. In earlier work these trajectories were found to be rather interesting. They showed that outside the region of adiabatic instabilities the expansion is adiabatic, i.e., the trajectories follow adiabats, etc.

The evolution trajectories of collision events are compared with those of disassembly of hot drops in Figs. 6 and 7. In 108 + 108 collisions both ρ_{ac} and T_{ac} increase with time immediately after the collision starts. During this interval there is no thermal equilibrium, and the beam energy is being converted into heat. After ~ 100 time steps from the start of collision the T_{ac} and ρ_{ac} begin to decrease, i.e., expansion cooling starts. Note that sound takes ~ 100 time steps to travel a distance equal to the radius of a 108-particle ball. At later times the evolution trajectories of 108 + 108 collisions are similar to those of the disassembly of hot drops having the same energy and an initial density of ~ 0.84 . The trajectories of 108 + 108 collisions at $e \sim 7.5$ pass above the adiabatic spinodal (curve labeled AS), and hence these events do not yield many fragments; however, many big fragments are created in 108 + 108 collisions at $e \sim 1$, presumably because their trajectories pass thru the region of adiabatic instabilities.

The trajectories of 200 + 16 collisions (Figs. 6 and 7) show that the maximum temperature reached in these events is much lower than 108 + 108 collisions occurring at the same center of mass energy. This is primarily due

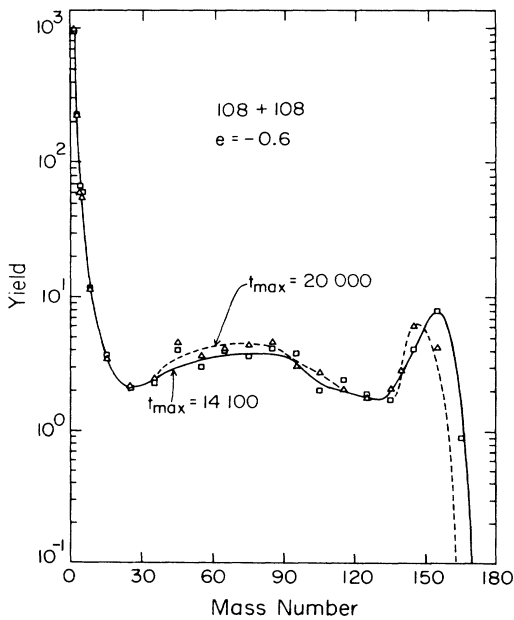


FIG. 8. Mass yield per 300 108 + 108 collisions at $e \approx -0.6$. The yields at $t = 14\,100$ and $20\,000$ are shown by squares and triangles, respectively.

to the large preequilibrium emission in these events. The 200 + 16 $e \sim 7.5$ trajectory at later times is similar to the 108 + 108 $e \sim 1$ trajectory, and hence the mass yield of 200 + 16 collisions at $e \sim 7.5$ is not too different from that of 108 + 108 collisions at $e \sim 1$. The compound system formed in the 200 + 16 collisions at $e \sim 1$ has very little energy. It expands only up to $\rho_{ac} = 0.56$, and either leaves an evaporation residue or fissions.

IV. MASS YIELDS

Molecular dynamics calculations can obviously be carried out only for a finite period of time evolution. In practice, the time t_{max} for which the system is evolved depends upon the energy, because systems with higher energy evolve faster. The calculation is stopped at a time t_{max} after all the "interesting phenomenon" are thought to have taken place and the rate of change has slowed down, as illustrated in Fig. 8. However, at t_{max} the larger clusters in the system still have enough excitation energy to evaporate many particles. Thus the mass yields at t_{max} would differ from the observed $t \rightarrow \infty$ asymptotic mass yields by this slow evaporation. Since the collision and disassembly events are evolved up to similar t_{max} , their comparison is not influenced by evaporation beyond t_{max} . The values of t_{max} used in this work are listed in Table I. All mass yields, energy spectra, and angular distributions discussed in this and subsequent sections are at t_{max} .

The mass yield per 300 108 + 108 collision events is shown in Fig. 9. The $e \sim -1$ mass yield has a narrow peak at $A = 170$ due to the evaporation residue of the fused system, a broad peak at $A \sim 85$ due to binary fission fragments, and an abundance of clusters with less than six

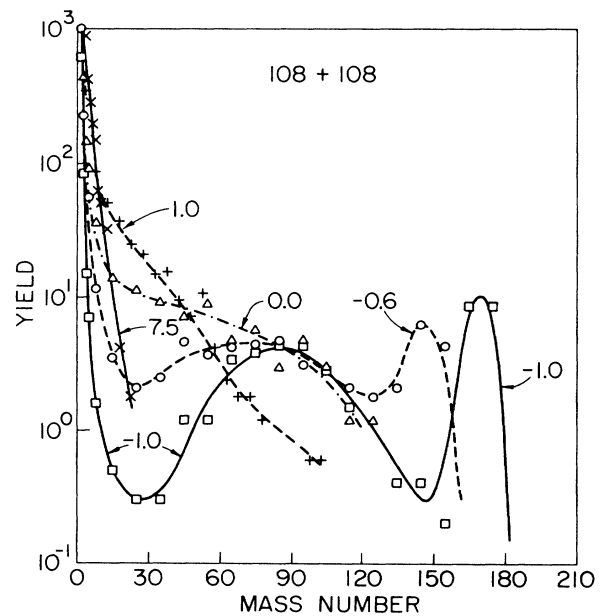


FIG. 9. Mass yield per 300 108 + 108 collisions. The curves are labeled with the average total energy e per particle, and the binned data at $e = -1, -0.6, 0.0, 1.0,$ and 7.5 are shown by squares, circles, triangles, + 's, and \times 's, respectively.

TABLE I. Values of t_{\max} in units of 10^{-14} s, for various events. The initial densities of disassembly events are given in parentheses.

e	$A = 216$			
	108 + 108	200 + 16	216 (0.84)	216 (1.2)
7.5	6000	6000	6000	6000
1.0	12 000	12 000	6000	6000
0.0	12 000	12 000	12 000	12 000
-0.6	20 000	20 000	12 000	12 000
-1.0	20 000	20 000	18 000	18 000

e	$A = 130$		
	65 + 65	130 (0.84)	130 (1.2)
4.7	6000	6000	6000
1.3	6000	6000	6000
0.2	12 000	12 000	6000
-0.7	20 000	18 000	18 000
-1.2	20 000	18 000	18 000

particles that have evaporated either from the compound system or the fission fragments. The fission fragments have approximately equal number of particles from the target and the projectile as illustrated in Figs. 1(a)–1(b). The valleys on both sides of the fission fragment peak are rather deep. As the energy is increased to $e \sim -0.6$ the evaporation residue peak shifts to lower mass values and becomes broader, the fission fragment peak also gets broader, and the valleys on its sides get filled up. At this energy the fission is mostly binary, and hence the filling of the valleys is due to more asymmetric fission. At $e = 0$ the mass yield becomes a monotonically decreasing function of mass, and we may consider it to be the beginning of fragmentation. At still higher energies the mass yield

becomes a rapidly decreasing function of mass; only $\sim 4\%$ of the events at $e \sim 7.5$ have a cluster with more than 20 particles in the final state. Thus this energy is near the end of the fragmentation region, as we expected from the evolution trajectories. Table II (III) lists events according to the number of clusters with $A > 20$ ($A > 10$) in the final state. The dependence of the probability of binary and multiple fission on the energy can be easily seen in these tables.

The mass yields observed in the disassembly of hot drops having 216 particles and an initial density of 0.84 and 1.2 are shown in Figs. 10 and 11. The mass yields are dependent on the initial density; systems with the same total energy produce more fragments when they have a lower entropy due to the large compressional ener-

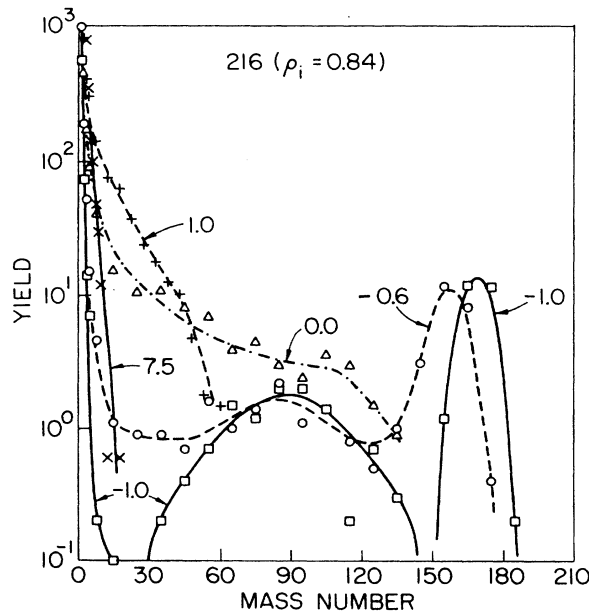


FIG. 10. Same as Fig. 9, except for disassemblies of 216-particle hot liquid drops from an initial density of 0.84.

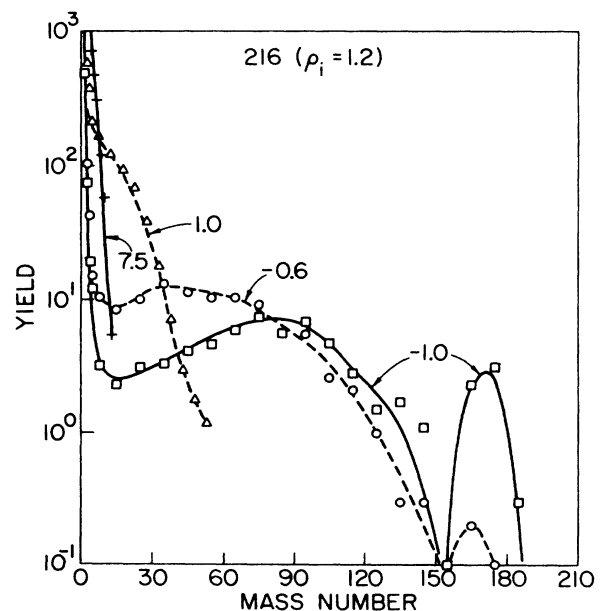


FIG. 11. Same as Fig. 10, except for initial density of 1.2.

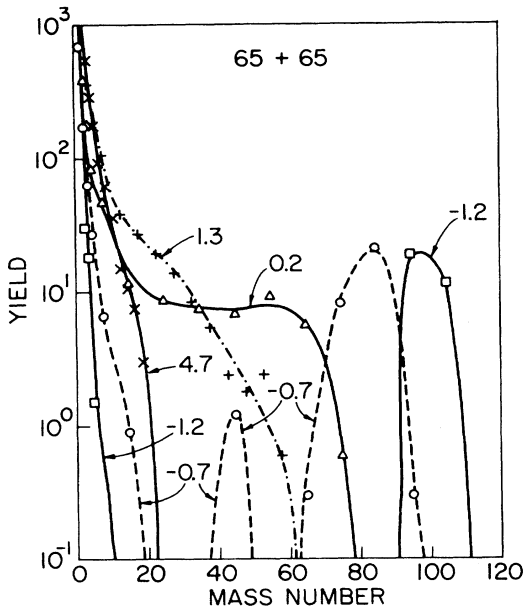


FIG. 12. Mass yields per 300 65 + 65 collisions. The curves are labeled with average total energy e per particle, and the binned data at $e = -1.2, -0.7, 0.2, 1.3,$ and 4.7 are shown by squares, circles, triangles, + 's, and \times 's, respectively.

gy. We note that the mass yield of 108 + 108 collisions is similar to that of disassembly events with $\rho_i = 0.84$ in the entire energy range considered here. This indicates that equilibrated hot matter at a density of ~ 0.84 is produced in these collisions. This density is less than the equilibrium density of cold matter ($= 1.04$).

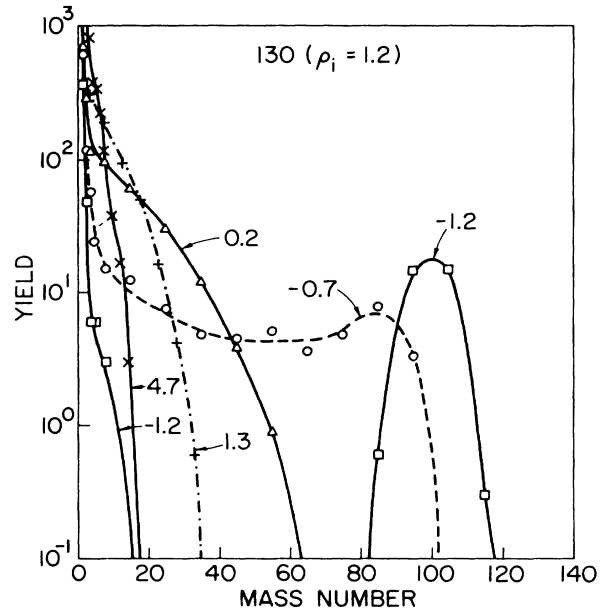


FIG. 14. Same as Fig. 12, except for initial density of 1.2.

The mass yields of 65 + 65 collisions are compared with those of the disassembly of 130 particle drops in Figs. 12–14. At $e \sim -1.2$ there is complete fusion in the collisions with no subsequent breakup, as can be seen from Fig. 12 and Table II. At $e \sim -0.7$ there is a small fission probability, while at $e \sim 4.7$ there is a small probability of finding clusters with $A > 20$ in the final state. The mass yield of the collisions is closer to that of

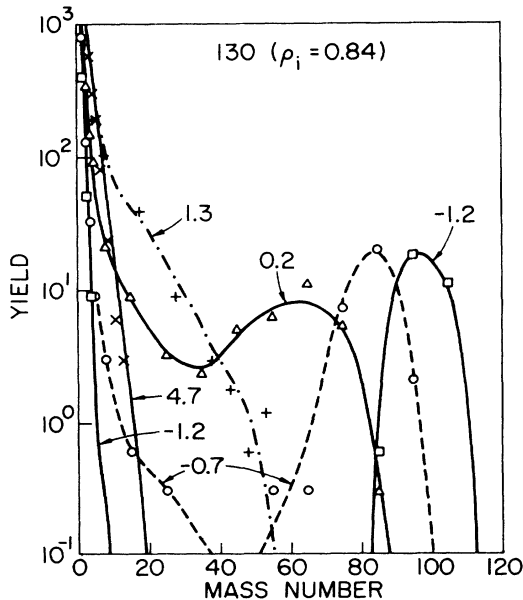


FIG. 13. Same as Fig. 12, except for disassemblies of 130-particle hot liquid drops from an initial density of 0.84.

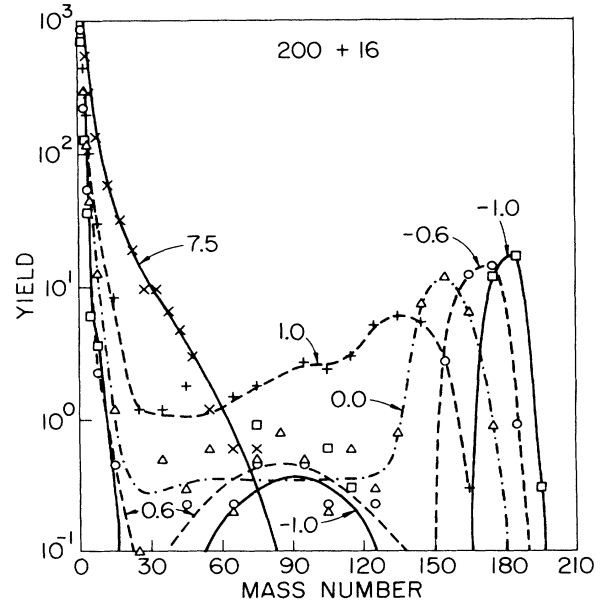


FIG. 15. Mass yields per 300 200 + 16 collisions. See caption of Fig. 9 for details.

disassembly from an initial density of 0.84, rather than 1.2.

The mass yield of collisions between 200- and 16-particle balls (Fig. 15) is rather different from that of disassembly of 108 + 108 collisions due to the large pre-equilibrium evaporation and energy loss. The evaporation residue peak persists up to $e \sim 1$, and the yield at $e \sim 7.5$ looks more like that due to fragmentation than vaporization.

V. ENERGY SPECTRA

In a hundred events many monomers and dimers are emitted, and it is possible to study their energy spectra. The number of emitted clusters having $A_c > 3$ (the number of particles in an emitted cluster is denoted by A_c),

however, is not sufficiently large. Hence we have grouped clusters with similar number of particles into mass bins to study their spectrum. These mass bins, the average kinetic energy due to center of mass motion of clusters emitted in the mass bin, and the fraction of particles in the mass bin are listed in Tables IV–VI for the 108 + 108, 65 + 65, and 200 + 16 collision events. Tables IV and V also report the average kinetic energies and mass fractions in 216- and 130-particle disassembly events with an initial density of 0.84. Some of the observed spectra are given in Figs. 16–22.

Apart from the effects of Coulomb repulsion at low energies, the spectra of monomers emitted in 108 + 108 and 65 + 65 collisions (Figs. 16 and 17) are approximately Maxwellian. However, the temperatures inferred from these spectra are rather large. For example, the apparent

TABLE II. The columns $M=0-5$ give the probability (%) for observing M clusters having 20 or more particles in the final state of a 108 + 108, 200 + 16, and 65 + 65 collision, and 216- and 130-particle disassembly. The initial densities of the disassembly events are given in parentheses.

Event	e	M					
		0	1	2	3	4	5
216 (1.2)	7.5	100					
216 (0.84)		100					
108+108		96	4				
200+16		19	61	17	3		
216 (1.2)	1.0	2	10	36	36	15	1
216 (0.84)		3	16	61	18	2	
108+108		20	56	22	2		
200+16			80	19	1		
216 (0.84)	0.0		28	47	21	4	
108+108			18	57	25		
200+16				93	7		
216 (1.2)	-0.6		2	36	47	14	1
216 (0.84)			78	21	1		
108+108			42	56	2		
200+16			97	3			
216 (1.2)	-1.0		20	66	13	1	
216 (0.84)			82	18			
108+108			58	42			
200+16			97	3			
130 (1.2)	4.7	100					
130 (0.84)		100					
65+65		98	2				
130 (1.2)	1.3	56	42	2			
130 (0.84)		33	58	8	1		
65+65		14	75	11			
130 (1.2)	0.2	2	36	50	10	2	
130 (0.84)			85	15			
65+65			69	30	1		
130 (1.2)	-0.7		61	35	4		
130 (0.84)			99	1			
65+65			98	2			
130 (1.2)	-1.2		100				
130 (0.84)			100				
65+65				100			

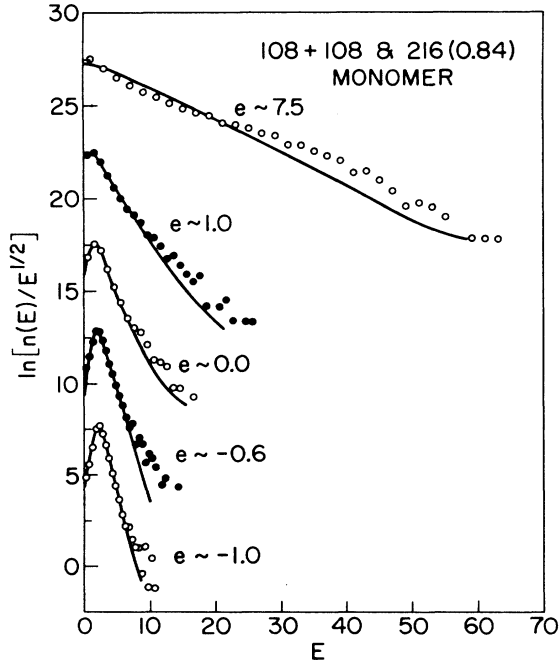


FIG. 16. The energy spectrum of monomers emitted in 108 + 108 collisions and disassemblies of 216 particles from $\rho_i = 0.84$. The data points show collision yields, while the curves give disassembly yields.

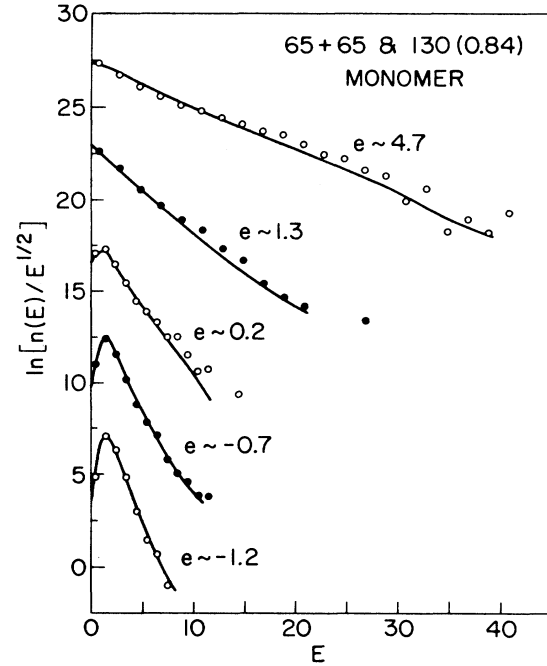


FIG. 17. Same as Fig. 16, except for 65 + 65 collisions and disassembly of 130 particles from $\rho_i = 0.84$.

temperature of monomers emitted in the 108 + 108 collisions at $e = 7.5$ is ~ 6.6 . This value is larger than the maximum temperature of 5.5 produced in these collisions as can be seen from the evolution trajectory (Fig. 7). The temperature of liquid having $e \sim 7.5$ and density 0.84 is 4.8, and the spectrum of monomers emitted in the disassembly of 216-particle drops at an initial density of 0.84 is similar to that observed in 108 + 108 collisions at

$e \sim 7.5$. The spectra of particles emitted in 216- and 130-particle disassembly events from $\rho_i = 0.84$ are also shown in Figs. 16 and 17. In general, they are very similar to those obtained in 108 + 108 and 65 + 65 collisions. As discussed in Ref. 10, the emission of monomers occurs throughout the disassembly during which the compound system is cooling; those emitted earlier have a large mean energy, while those emitted later have a much smaller

TABLE III. The columns $M = 0-6$ give the probability (%) for observing M clusters having 10 or more particles in the final state of collisions.

Event	e	M						
		0	1	2	3	4	5	6
108 + 108	7.5	36	51	9	4			
	1.0		2	14	37	22	21	4
	0.0		8	37	45	9	1	
	-0.6		33	58	9			
	-1.0		57	42	1			
200 + 16	7.5		9	26	53	10	2	
	1.0		59	33	6	2		
	0.0		88	12				
	-0.6		95	5				
	-1.0		97	3				
65 + 65	4.7	37	56	7				
	1.3		21	45	26	8		
	0.2		36	54	9	1		
	0.7		95	5				
	-1.2		100					

mean energy. Thus the approximate Maxwellian nature of the monomer spectrum probably has a complex origin, and it does not reflect the temperature of the compound system at any time during the collision or disassembly. The spectra of monomers emitted in the $200 + 16$ collisions (Fig. 18) are much less Maxwellian than of those emitted in either equal mass collisions or disassemblies due to preequilibrium emission.

The kinetic energy spectrum of clusters of various mass are shown in Figs. 19–22. In equal mass collisions and disassemblies, the average kinetic energy of the emitted dimers and light ($A_c < 10$) clusters increases with A_c , and their spectrum appears to be approximately Maxwellian.

If the kinetic energies have a dominant contribution from the flow velocity of expanding matter, we expect the light clusters to have the same velocity, and their average kinetic energies to be proportional to A_c . The kinetic energies due to Coulomb repulsion are also expected to be proportional to A_c for small clusters. On the other hand, if all the emitted clusters have only thermal velocities, then their kinetic energies would be independent of A_c . The results suggest that when $e = 7.5$ clusters with two or more particles emitted in $108 + 108$ collisions have similar average energies, and their spectra (Fig. 20) are approximately Maxwellian with an apparent temperature of 11 K. This temperature is again much larger than that of

TABLE IV. The average kinetic energy of the clusters emitted in $108 + 108$ collisions and disassemblies of 216-particle drops from an initial density of 0.84, at various values of e . The fraction of particles in the initial state that is emitted in clusters of various mass is also listed.

e	Cluster size	Avg. cluster energy		Particle fraction	
		108 + 108	216	108 + 108	216
7.5	1	9.92	9.09	0.538	0.615
	2	15.51	12.21	0.162	0.180
	3–5	16.55	13.97	0.177	0.168
	6–10	18.07	17.91	0.083	0.036
	11–20	14.29	20.58	0.037	0.001
1.0	1	3.01	2.94	0.349	0.323
	2	6.03	4.67	0.080	0.072
	3–5	9.06	6.70	0.079	0.086
	6–10	13.62	10.06	0.050	0.084
	11–20	16.12	13.84	0.102	0.162
	21–30	17.13	16.34	0.089	0.118
0.0	31–60	12.43	18.11	0.204	0.151
	1	2.51	2.49	0.321	0.309
	2	4.80	4.02	0.047	0.051
	3–5	7.48	6.03	0.037	0.038
	6–10	11.36	10.50	0.022	0.024
	11–30	17.06	15.62	0.078	0.077
	31–60	17.53	17.08	0.175	0.177
–0.6	61–90	11.99	11.87	0.156	0.132
	91–120	4.44	5.01	0.141	0.143
	1	2.48	2.53	0.245	0.217
	2	4.36	3.99	0.031	0.031
	3–5	6.41	5.73	0.019	0.013
	6–10	10.05	9.73	0.007	0.003
	11–30	37.82	15.43	0.016	0.006
	31–60	20.87	15.42	0.078	0.024
–1.0	61–90	16.77	14.07	0.158	0.055
	91–120	10.88	9.38	0.127	0.053
	130–160	1.52	1.33	0.289	0.372
	161–180		0.79		0.216
	1	2.52	2.55	0.183	0.189
	2	4.18	4.05	0.019	0.017
	3–5	5.89	6.00	0.005	0.005
–1.0	31–60	22.87	21.38	0.021	0.010
	61–90	18.94	18.25	0.137	0.056
	91–120	15.20	12.46	0.135	0.055
	121–150	7.79	7.49	0.040	0.020
	150–180	0.66	0.60	0.457	0.642

the compound system. On the other hand, at the lowest energy [$e = -1$ for $108 + 108$ or $B(216)$] the energies of monomers, dimers, and clusters with $3 < A_c < 5$ are influenced by Coulomb forces. The average energy of light clusters increases, though not quite linearly, with A_c .

The spectra of heavy clusters are not Maxwellian. Their kinetic energies appear to be dominated by Coulomb forces. For example, the two fission fragments having $A_c \sim 85$, emitted in $108 + 108$ collisions, separate from each other when their centers are ~ 10 units apart [Figs. 1(d) and 1(e)]. Their Coulomb energy at scission is ~ 20 units per fragment. Thus the Coulomb repulsion accounts for the observed average energy of clusters with 61–90 particles emitted in events with $e < 0$. A significant fraction of the kinetic energies of the 20- to 60-particle fragments, emitted in the $e = 1$ events, should also be due to Coulomb repulsion.

VI. ANGULAR DISTRIBUTIONS

Angular distributions observed in $108 + 108$ collisions at $e = -1, 0$, and 7.5 are shown in Figs. 23–26, while those observed in $65 + 65$ collisions are shown in Figs. 27–29 and those for $200 + 16$ collisions at $e = 0$ are in Figs. 30 and 31. All of these angular distributions are in the center of mass frame, and those of symmetric col-

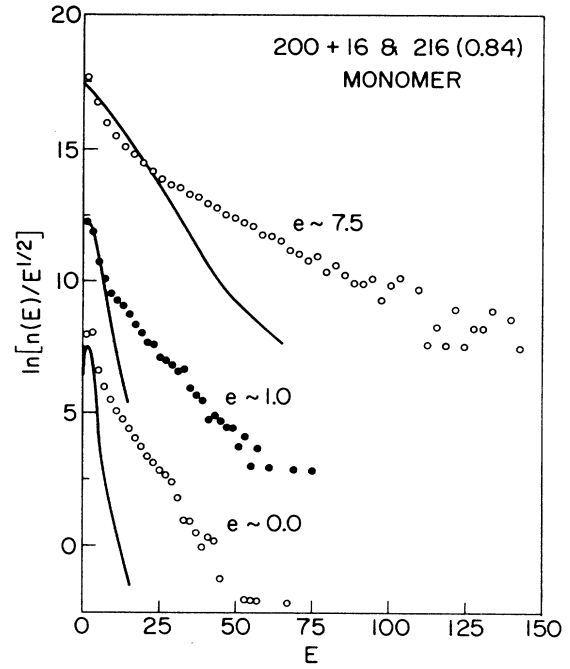


FIG. 18. Same as Fig. 16, except for $200 + 16$ collisions and disassembly of 216 particles from $\rho_i = 0.84$.

TABLE V. Same as Table IV, except for $65 + 65$ collisions and disassemblies of 130-particle drops from an initial density of 0.84.

e	Cluster size	Avg. cluster energy		Particle fraction	
		65 + 65	130	65 + 65	130
4.7	1	6.54	6.23	0.502	0.555
	2	10.38	7.96	0.164	0.175
	3–5	11.50	9.74	0.187	0.194
	6–10	11.63	11.32	0.093	0.071
	11–20	8.72	9.73	0.054	0.005
1.3	1	3.11	2.97	0.351	0.361
	2	5.38	4.04	0.096	0.091
	3–5	6.98	5.78	0.115	0.116
	6–10	8.52	7.35	0.103	0.103
	11–20	8.82	8.88	0.125	0.175
	21–30	6.93	7.96	0.105	0.088
0.2	31–60	5.15	7.10	0.105	0.066
	1	2.19	2.18	0.341	0.339
	2	3.86	3.13	0.067	0.064
	3–5	5.61	4.63	0.060	0.054
	6–10	7.86	6.77	0.046	0.021
	11–20	8.93	7.90	0.046	0.035
	21–40	7.98	9.96	0.125	0.042
-0.7	41–60	3.18	4.19	0.212	0.150
	61–80	2.16	1.67	0.104	0.289
	1	2.04	2.11	0.299	0.299
	2	3.28	3.10	0.036	0.041
	3–5	4.80	4.04	0.023	0.015
-1.2	61–100	0.90	0.85	0.620	0.633
	1	2.02	2.06	0.206	0.210
	2	3.16	3.13	0.021	0.020
	86–110	0.60	0.56	0.768	0.765

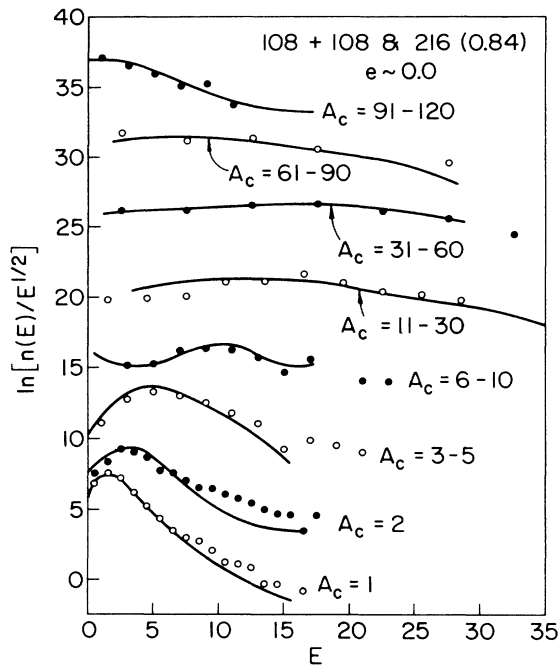


FIG. 19. The energy spectra of clusters emitted in 108 + 108 collisions (data points) and disassemblies of 216 particles from $\rho_i = 0.84$ (solid lines), both at $e \sim 0$. The data is labeled with A_c bin sizes, and the internal excitation energies of clusters are not included.

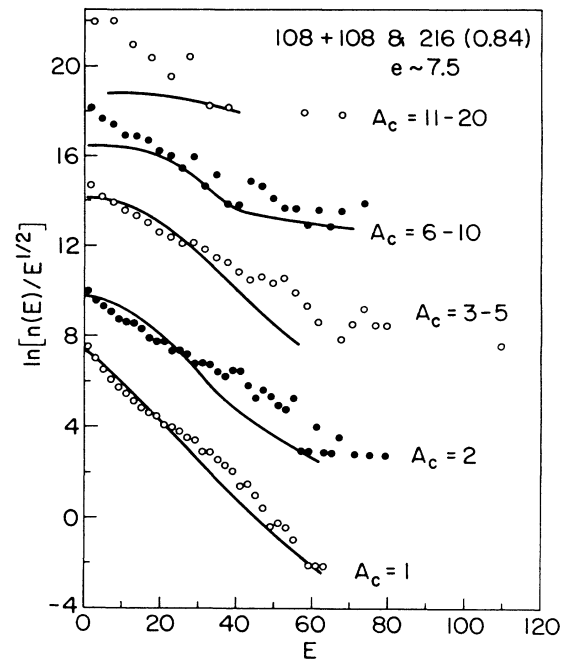


FIG. 20. Same as Fig. 19, except at $e \sim 7.5$.

TABLE VI. Same as Table IV, except for 200 + 16 collisions.

e	Cluster size	Avg. cluster energy	Particle fraction
7.5	1	14.11	0.456
	2	14.97	0.105
	3-5	12.97	0.111
	6-10	14.17	0.076
	11-20	14.46	0.103
	21-30	15.38	0.054
	31-60	8.63	0.081
1.0	1	6.70	0.259
	2	10.84	0.051
	3-5	11.60	0.041
	6-10	13.11	0.017
	11-30	18.42	0.023
	31-60	17.20	0.023
	61-90	11.36	0.037
	91-120	6.14	0.133
121-170	2.61	0.416	
0.0	1	5.72	0.213
	2	10.11	0.037
	3-5	11.26	0.025
	6-10	13.58	0.007
	11-30	17.33	0.003
	31-60	21.96	0.010
	61-90	15.37	0.019
	91-120	9.17	0.021
	121-150	2.22	0.192
	151-180	1.66	0.475

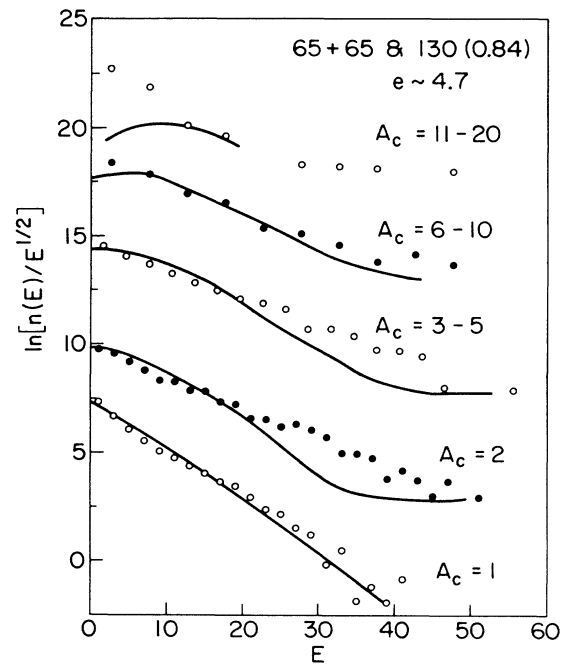


FIG. 21. Same as Fig. 19, except for 65 + 65 collisions and 130-particle disassemblies at $e \sim 4.7$.

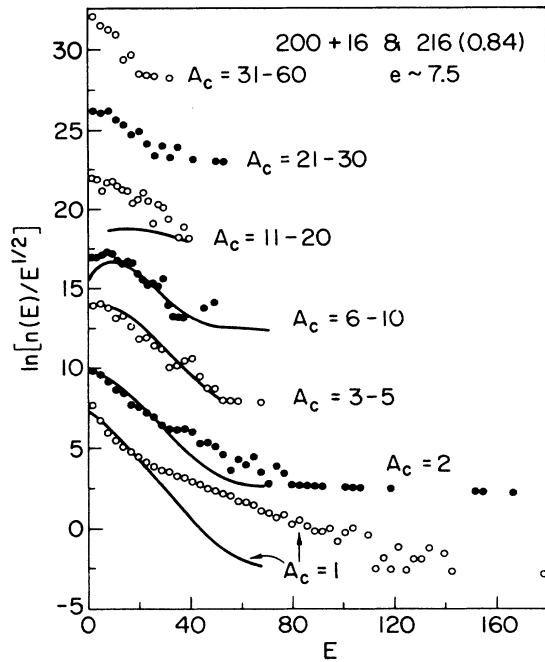


FIG. 22. Same as Fig. 19, except for 200 + 16 collisions and 216-particle disassemblies at $e \sim 7.5$.

lisions are symmetric about 90° . The angular distribution $dn(A_1, A_2, A_c, e)/d\Omega$ depends on A_1, A_2, A_c , and e , and it is normalized so that

$$\int \frac{dn}{d\Omega} d\Omega = 1. \quad (6.1)$$

In symmetric collisions the angular distribution of mono-

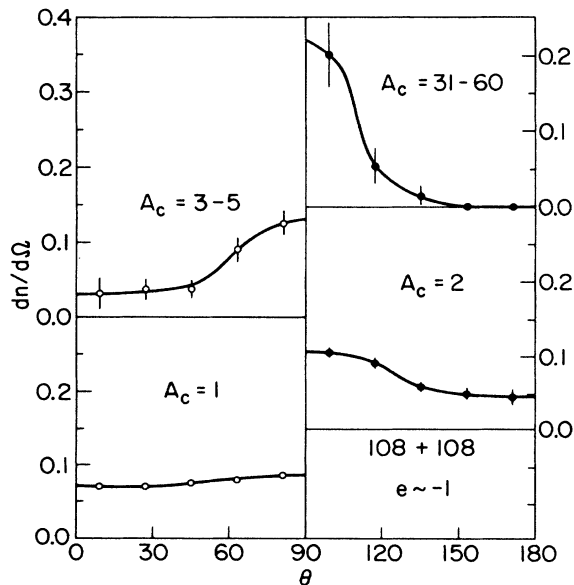


FIG. 23. Angular distributions of clusters emitted in 108 + 108 collisions at $e \sim -1$. Note that $dn/d\Omega = 0.08$ for isotropic distribution.

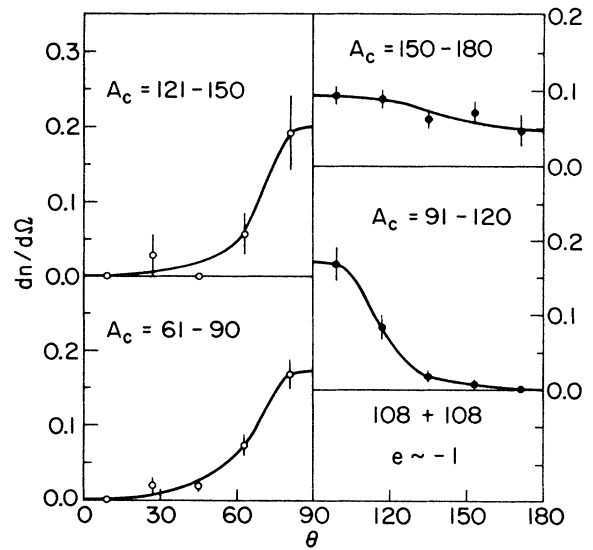


FIG. 24. Same as Fig. 23, except for different values of A_c .

mers is almost isotropic at lower energies, and it becomes transverse peaked as the energy of collision increases. This can be most clearly seen in Fig. 27, which gives the monomer distributions in 65 + 65 collisions at various energies. It can also be seen by comparing monomer distributions in Figs. 23, 25, and 26 for 108 + 108 collisions. The 65 + 65 collisions at $e = -1.2$ and -0.7 as well as the 108 + 108 collisions at $e = 1$ produce fusion followed

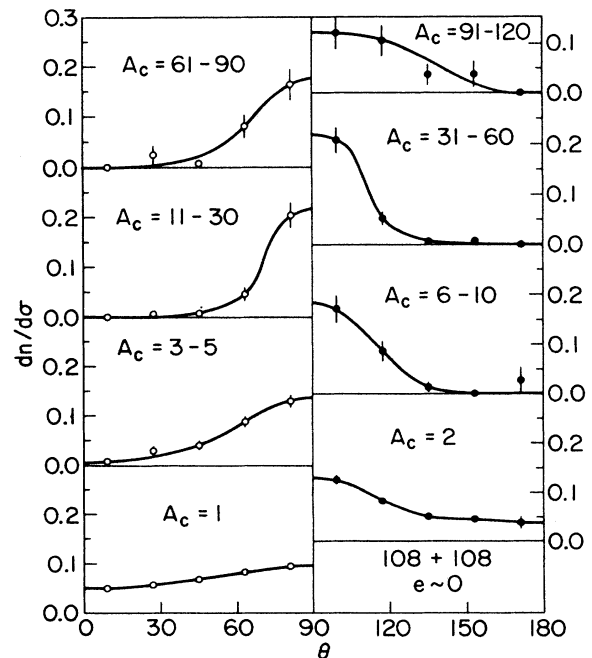


FIG. 25. Same as Fig. 23, except for 108 + 108 collisions at $e \sim 0.0$.

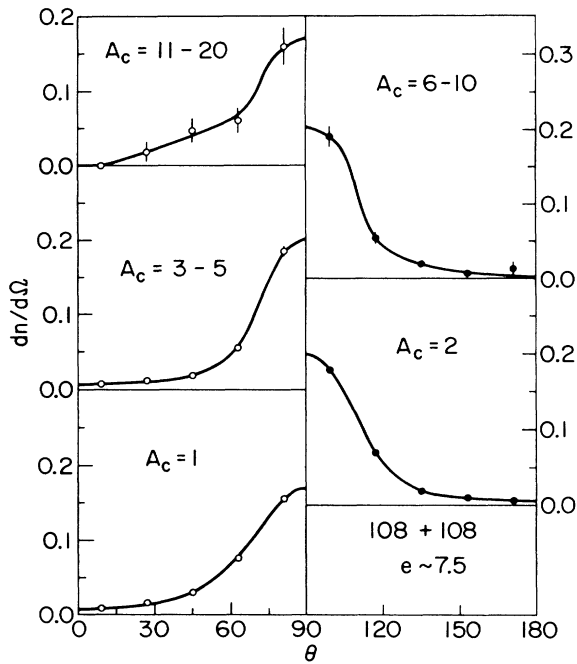


FIG. 26. Same as Fig. 23, except for 108 + 108 collisions at $e \sim 7.5$.

by evaporation or fission. The monomers emitted in these events are due to almost isotropic evaporation. However, even at these low energies light clusters having 3–5 particles are emitted preferentially transversely. The fission fragments having 30–150 particles are also emitted, mostly in the $\theta = 45^\circ - 135^\circ$ range with a peak at 90° (Figs. 23

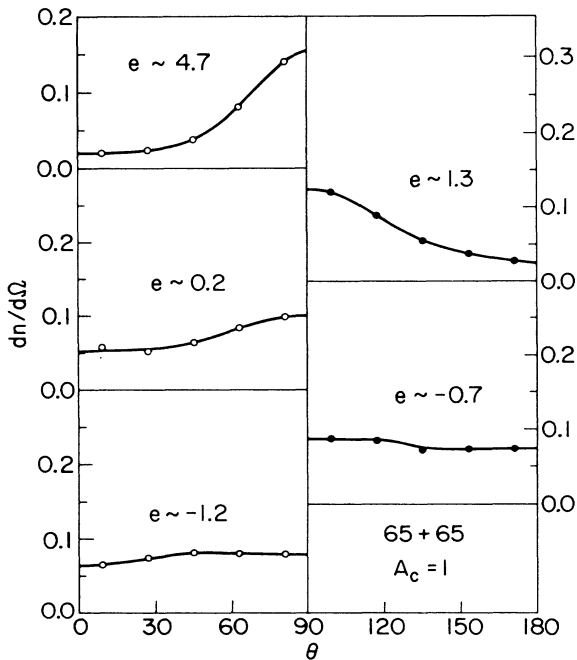


FIG. 27. The angular distribution of monomers emitted in 65 + 65 collisions at various energies.

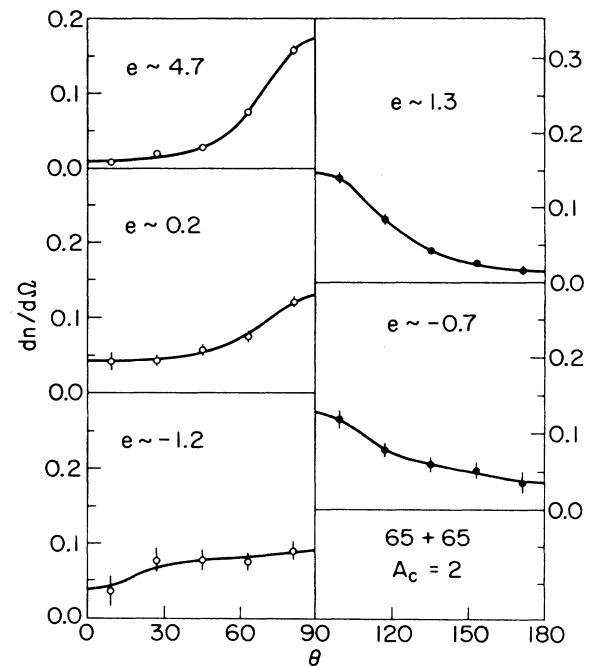


FIG. 28. The angular distribution of dimers emitted in 65 + 65 collisions at various energies.

and 24). This transverse peaking of light and heavy clusters is probably due to the pancake-like deformed shape of the compound system as can be seen in Figs. 1(a)–1(e) and 2(a)–2(c). The evaporation residues ($A_c = 150 - 180$ in Fig. 23), however, have fairly isotropic angular distribution.

In fragmentation events ($e \sim 0$ for 108 + 108 and $e = 0.2$ and 1.3 for 65 + 65) the angular distributions of

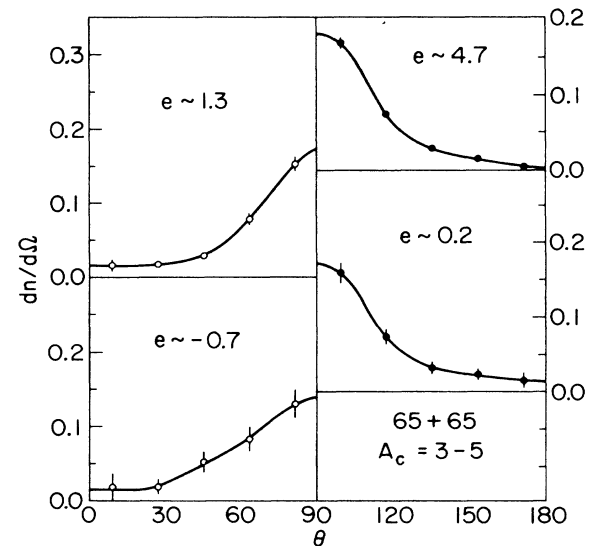


FIG. 29. The angular distribution of clusters having 3, 4, and 5 particles, emitted in 65 + 65 collisions at various energies.

all clusters show transverse peaking. However, the monomers and dimers have an appreciable isotropic component, whereas the yield of clusters with more than three particles is very small in forward and backward directions. Particularly in $108 + 108$ collisions at $e \sim 0$, we obtain essentially zero yield of $A_c \geq 3$ clusters in the $\theta = 0^\circ - 18^\circ$ and $162^\circ - 180^\circ$ bins. In the high energy total vaporization event ($e = 7.5$, $108 + 108$, Fig. 25) all yields are transverse.

The yields in the asymmetric $16 + 200$ collisions (Figs. 30 and 31) have rather interesting angular distributions. The monomer and dimer yields are approximately symmetric about 90° , and show some transverse peaking at $e = 0$. The yields of light clusters with 6–30 particles are shifted to larger angles, while those of heavy ($A_c > 90$) fragments are peaked at 0° . Note that before collision the 16- (200-) body cluster is moving in the 180° (0°) direction.

VII. CONCLUSIONS

The present calculations indicate that hot matter is formed in head on collisions between two equal mass cold clusters having ~ 100 particles. It appears that, in the energy domain studied, the density of the hot matter formed in the collisions is ~ 0.84 , or $\sim 20\%$ less than the equilibrium density. Its temperature can be varied by changing the beam energy. In equal mass collisions all the beam energy seems to thermalize; in contrast, in the $200 + 16$ collisions there is a large preequilibrium emission. The problem of calculating mass yields and energy distributions in collisions between two equal mass atomic clusters can thus be simplified considerably by assuming the for-

mation of a hot liquid drop. However, the angular distribution of the matter emitted in collisions is strongly correlated with the beam axis, whereas that emitted by the hot drops is isotropic. The hot drops formed in the collisions are not good examples of "compound nuclei"; they retain the memory of beam axis.

The mass yields and energy distributions of the final state depend upon the initial density ρ_i and temperature T_i of the hot matter. Thus, in principle, it is possible to deduce the ρ_i and T_i of the hot matter formed in the collisions from the observed mass yields and energy distributions, and measure the equation of state $e(\rho_i, T_i)$. Unfortunately, a practical method of inferring ρ_i and T_i from the final state is not yet available. The apparent temperature of the monomers emitted in collisions as well as disassemblies is much larger than T_i .

The boundary between vaporization and fragmentation is determined by the location of the evolution trajectory with respect to the adiabatic spinodal (AS) curve. Large fragments are produced in events whose trajectories pass through the region of instabilities enclosed by the AS. Thus the liquid-gas phase transition has an effect on the dynamics of systems even when they contain only ~ 100 particles.

The yield of fragments with mass $A_c \ll A$ emitted in nuclear fragmentation reactions^{1-3,14,15} is often fitted to a simple power law:

$$Y(A_c) = Y_0 A_c^{-\tau_{\text{eff}}} . \quad (7.1)$$

The yield of fragments having $A_c \sim A$ comes from either evaporation residues or fission, and it obviously depends upon the mass A of the compound system. The power

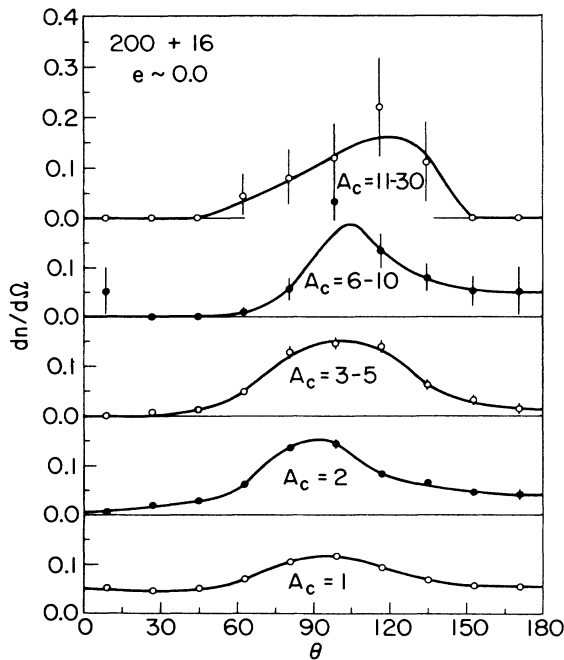


FIG. 30. The angular distribution of clusters emitted in $200 + 16$ collisions at $e \sim 0.0$.

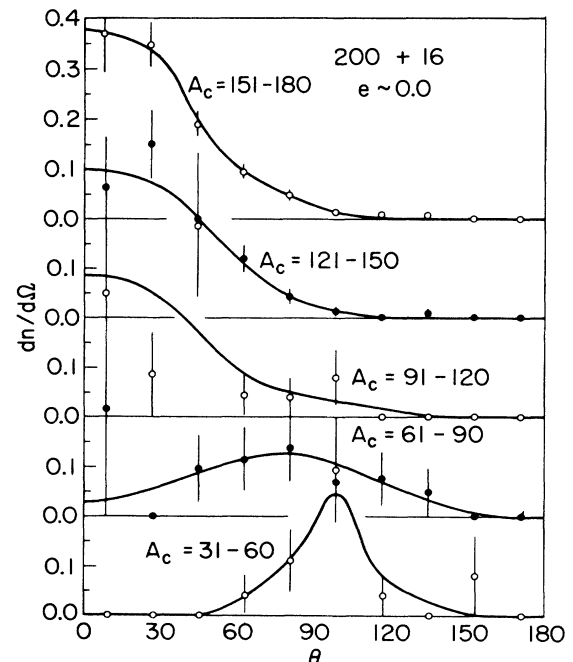


FIG. 31. Same as Fig. 30, except for different values of A_c .

law (7.1) has been inspired by the work of Fisher,¹⁶ who showed that the abundance of clusters in extended matter near the critical point ($T, \rho \sim T_c, \rho_c$) is proportional to $A_c^{-\tau}$, where τ is expected to be between 2 and 3; it is $\frac{7}{3}$ is mean field theory.¹⁵

Power-law fits to our mass yields are shown in Figs. 32 and 33. In 108 + 108 collisions at lower energies the mass yield has a minimum at $A_c \sim 30$ (Fig. 9) which arises due to fission. Thus the power law can only be used at $A_c < 30$. In these collisions (Fig. 32) larger values of τ_{eff} are obtained when the yields of masses in the region $4 \leq A_c \leq 10$ are fitted by the power law than when the region $4 \leq A_c \leq 30$ is used. In 65 + 65 collisions, on the other hand, the yields in the region $4 \leq A_c \leq 30$ can be fitted by the power law within the accuracy of the data (Fig. 33).

We note that the values of τ_{eff} do not depend significantly on the mass of the compound system; however, they do depend upon the energy of the collision. Thus they may contain useful information. The τ_{eff} has a minimum value of ~ 1.7 at $e \sim 0$. The evolution trajectories of some of the events are shown in Fig. 34. All along these trajectories there exists a single compound system. The trajectories in Fig. 34 end when the compound system has developed significant inhomogeneities or surface deformations. Thus their end points crudely mark the region in which matter fragments or fissions. We see that the matter produced in collisions at $e \sim 4.7-7.5$ passes through the critical region

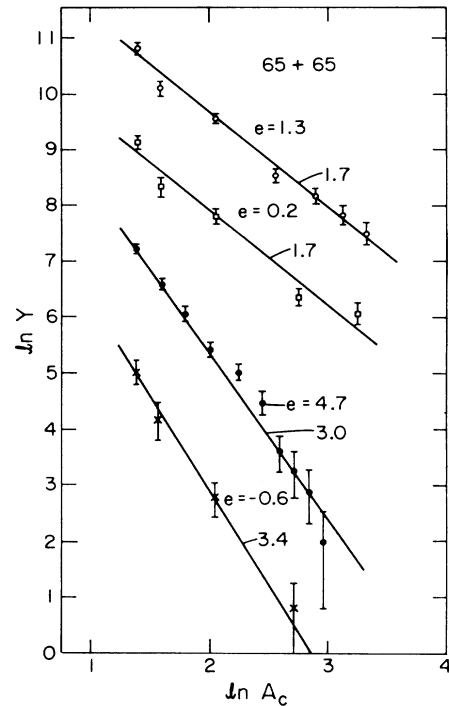


FIG. 33. Same as Fig. 32 for 65 + 65 collisions.

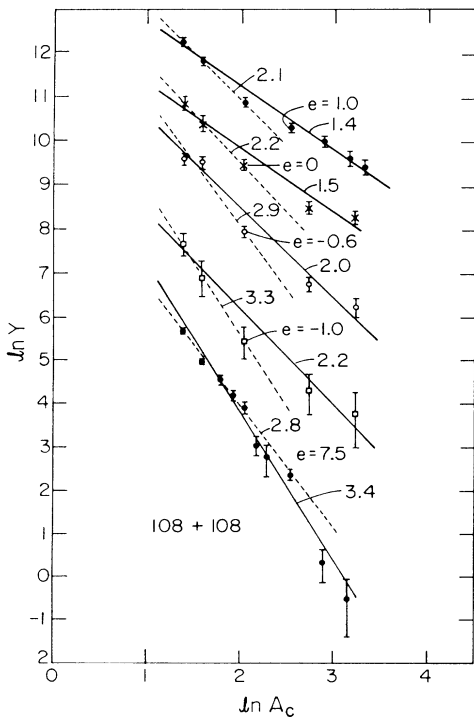


FIG. 32. Power-law fits to mass yields in 108 + 108 collisions. The lines are labeled with their slope τ_{eff} .

($T, \rho \sim T_c, \rho_c$), but it fragments at much lower density and temperature with a $\tau_{\text{eff}} \gtrsim 3$. The matter produced in collisions at $e \sim -0.1-1.3$ expands and fragments in the region of adiabatic instabilities at $\rho \sim 0.3$ with a $\tau_{\text{eff}} \sim 1.7$. The matter in the low energy ($e \sim -1$) collisions does not fragment. It stays at a density close to the liquid density, and the yields of these events have either evaporation residue or fission fragments. The small A_c yield at $e \sim -1$ comes via evaporation, and has $\tau_{\text{eff}} \gtrsim 3$.

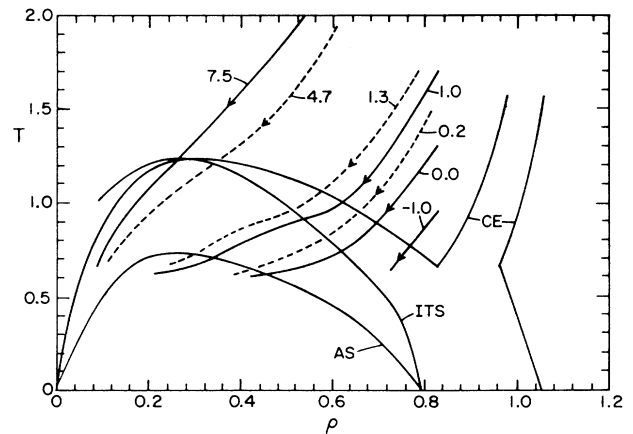


FIG. 34. Evolution trajectories of central matter in 108 + 108 (solid lines) and 65 + 65 (dashed lines) collisions. The trajectories are labeled with e .

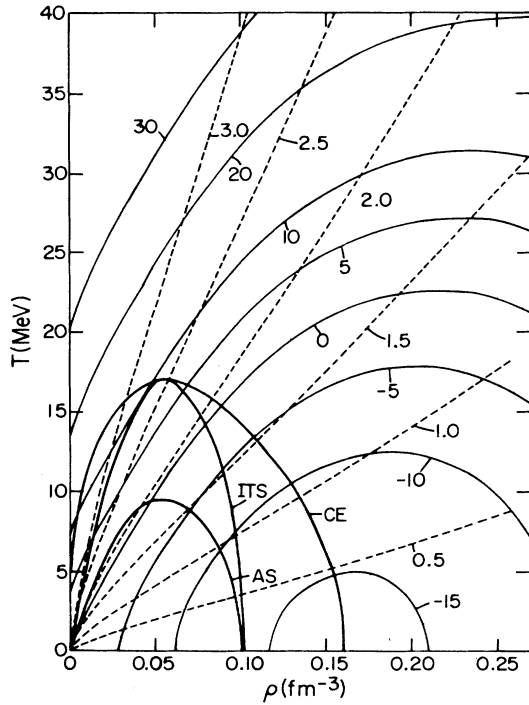


FIG. 35. A theoretically predicted phase diagram of nuclear matter showing the coexistence curve (CE), ITS, and AS. Dashed lines labeled with entropy give the adiabats, while solid lines give the internal energy per nucleon.

The minimum value of τ_{eff} in nuclear fragmentation reactions¹⁴ is also ~ 1.7 , as seen in p + U collisions^{17,18} at ~ 5 GeV. It is possible that only $\sim 25\%$ of the beam energy is thermalized among ~ 200 nucleons in these events. The compound system will then have an energy $e \sim 0$, and initial density $\rho_i \sim 0.16 \text{ fm}^{-3}$. From the phase diagram of nuclear matter^{19,20} (Fig. 35) it appears that the evolution trajectory of matter having $e \sim 0$, adiabatically expanding from $\rho_i \sim 0.16 \text{ fm}^{-3}$, will also pass through the top region of adiabatic instabilities. Such matter will have an initial temperature of ~ 20 MeV, and it will fragment at a temperature of about 5–7 MeV.

The fragmentation of hot matter, as observed in these classical simulations of collisions and disassemblies, is similar to that assumed by the Purdue-Fermilab collaboration¹ in the analysis of their data. However, there are two

differences. First, they assume that an observation of $A_c^{-\tau_{\text{eff}}}$ power-law mass yield at small A_c implies that the fragmentation took place near the critical temperature T_c . We find that the mass yields at small A_c have a power-law behavior even when fragmentation occurs at temperatures much below T_c . This is particularly true for the $A = 130$ systems in which fission is not dominant. Also the smallest value of τ_{eff} occurs at $e \sim 0$, and not when the expanding system passes thru the critical region, $T, \rho \sim T_c, \rho_c$. Second, both in our simulations and in the Purdue-Fermilab experiments the mean kinetic energy, or the apparent temperature, of the fragments is much larger than that of the system. Their interpretation is that the fragment kinetic energies are influenced by the Fermi motion of nucleons. There is no Fermi motion in our classical system; the large kinetic energies of fragments in our simulations appear to come from collective motion of expansion and Coulomb repulsion.

The abundance of fragments of mass A_c in charge neutral matter in thermodynamic equilibrium at $T < T_c$ is given by the droplet model:^{1,15,16}

$$Y(A_c) = Y_0 A_c^{-\tau_{\text{eff}}} \exp[-\beta(a_v A_c + a_s(T) A_c^{2/3})]. \quad (7.2)$$

The volume coefficient a_v equals the difference between the chemical potentials in gas and liquid phase, and it must be zero in equilibrium. At $T = T_c$ we obtain the power law (7.1) because the surface coefficient $a_s(T_c) = 0$. At $T < T_c$, however, $a_s(T)$ can be greater than 0. The present $A = 130$ mass yields at small A_c (Fig. 33) can be explained just with the power law. The statistical errors in the calculation will have to be reduced by simulating thousands of events to study the nature of the exponential term in $Y(A_c)$. The $A = 216$ ($108 + 108$ yields in Fig. 9) have a minimum at $A_c \sim 30$ at $e = -1$ and -0.6 . This minimum is similar to that observed in low energy carbon on gold experiments,² and it can be reproduced by letting $a_v < 0$ as discussed in Ref. 15. However, this minimum occurs due to fission, which is not at all considered in arriving at Eq. (7.2).

ACKNOWLEDGMENTS

The authors wish to thank Professor D. G. Ravenhall and Mr. R. J. Lenk for many discussions. The simulations were carried out on the Cray-XMP computer of the National Center for Supercomputing Applications at Urbana-Champaign. This work was supported by the U.S. National Science Foundation under Grant PHY84-15064.

¹J. E. Finn *et al.*, Phys. Rev. Lett. **49**, 1321 (1982); R. W. Minisch *et al.*, Phys. Lett. **118B**, 458 (1982); A. S. Hirsch *et al.*, Phys. Rev. C **29**, 508 (1984).

²C. B. Chitwood *et al.*, Phys. Lett. **131B**, 289 (1983).

³A. I. Warwic *et al.*, Phys. Rev. C **27**, 1083 (1983).

⁴J. Knoll and B. Strack, Phys. Lett. **149B**, 45 (1984).

⁵S. Das Gupta, C. Gale, and J. Gallego, Phys. Rev. C **33**, 1634 (1986); S. Das Gupta *et al.* (unpublished).

⁶D. H. Boal, University of Illinois Report P/86/5/77, 1986.

⁷G. F. Bertsch, H. Kruse, and S. Das Gupta, Phys. Rev. C **29**,

- 673 (1984).
- ⁸G. F. Bertsch and P. J. Siemens, Phys. Lett. **126B**, 9 (1983).
- ⁹J. A. Lopez and P. J. Siemens, Nucl. Phys. **A431**, 728 (1984).
- ¹⁰A. Vicentini, G. Jacucci, and V. R. Pandharipande, Phys. Rev. C **31**, 1783 (1985).
- ¹¹R. J. Lenk and V. R. Pandharipande, Phys. Rev. C **34**, 177 (1986).
- ¹²D. J. E. Callaway, L. Wilets, and Y. Yariv, Nucl. Phys. **A327**, 250 (1979).
- ¹³A. R. Bodmer, C. N. Panos, and A. D. MacKeller, Phys. Rev. C **22**, 1025 (1980).
- ¹⁴A. D. Panagiotou *et al.*, Phys. Rev. Lett. **52**, 496 (1984).
- ¹⁵A. L. Goodman, J. I. Kapusta, and A. Z. Mekjian, Phys. Rev. C **30**, 851 (1984).
- ¹⁶M. E. Fisher, Physica (N.Y.) **3**, 255 (1967).
- ¹⁷G. D. Westfall *et al.*, Phys. Rev. C **17**, 1368 (1978).
- ¹⁸A. M. Poskanzer, G. W. Butler, and E. K. Hyde, Phys. Rev. C **3**, 882 (1971).
- ¹⁹B. Friedman and V. R. Pandharipande, Nucl. Phys. **A361**, 502 (1981).
- ²⁰D. G. Ravenhall, private communication.